Microwave Solid-State Synthesis of LiV_3O_8 as Cathode Material for Lithium Batteries

Gang Yang,[†] Guan Wang,[‡] and Wenhua Hou*[,†]

Key Laboratory of Mesoscopic Chemistry of MOE, School of Chemistry and Chemical Engineering, Nanjing University, Nanjing 210093, People's Republic of China, and Department of Chemistry, Fudan University, Shanghai 200433, People's Republic of China

Received: January 25, 2005; In Final Form: March 3, 2005

A novel and economical microwave route has been developed for the synthesis of electrochemically active LiV_3O_8 material by using a domestic microwave oven. The heating behavior of the designed reaction system guided the preparation of LiV_3O_8 at a suitable irradiation power (i.e. heating rate), reaction time, and temperature. At the lowest irradiation power, the conversion fraction of reactants was mainly controlled by reaction temperature. Characterization results of X-ray diffraction (XRD), Fourier transform infrared (FTIR) and Raman spectroscopy, scanning (SEM) and transmission (TEM) electron microcopy, and BET surface areas indicated that the phases of samples prepared by microwave and traditional methods were in good agreement. Nevertheless, the crystallinity, crystallite configuration, and morphology of the samples were different, and were affected by the irradiation time and power. A floppy superposition structure of nanosheets (the size of one nanosheet was about 4.5 μm × 1.2 μm × 3 nm) was preferentially grown at the lowest irradiation power, and this effect on structure was more in evidence as the nanorods formed at the highest irradiation power. Electrochemical studies on ionic conductivity, electrochemical impedance spectroscopy (EIS), and charge−discharge capacity were carried out. It was found that the conductivity, first discharge capacity, and cycle performances of the samples were affected by the crystal size, crystallinity, and crystal configuration and defection concentration. The sample L30 prepared at the lowest irradiation power and the shortest time (30 min) showed the highest discharge capacity (335 mAh/g), but its discharge capacity decreased rapidly. By comparison, the sample L100 had a floppy superposition structure of nanosheets and a high surface area, provided a good two-dimensional channel for the transition of Li^+ ions, and was stable during the intercalation/deintercalation process of Li^+ ions, therefore the high ionic conductivity, high discharge capacity, and good cycle performance were presented. The relationship between the electrochemical properties and the irradiation power was discussed.

1. Introduction

Significant effort has been made on the development of rechargeable cathode materials for secondary lithium batteries. LiV_3O_8 has been widely studied for about 20 years due to its high capacity, facile preparation, and stability in air. In fact, it is one of the promising substitutes for the expensive and toxic cathode material of $LiCoO_2$.[1−4] In the early development, Nassau and Murphy[3] realized that the preparation method of LiV_3O_8 strongly influenced its electrochemical properties, such as discharge capacity, rate capacity, and cycle performances. Since then, a great deal of research has been focused on the preparation methods (e.g., hydrothermal, sol−gel, lower temperature synthesis, and so forth) to enhance the electrochemical behavior.[4−10] Traditional synthesis of LiV_3O_8 is carried out by reacting Li_2CO_3 and V_2O_5 at 680 °C for 10 h.[11] This method usually produces sintered LiV_3O_8. Moreover, to improve the electrochemical performance of LiV_3O_8, many succeeding treatments have been proposed, such as efficient grinding, rapid cooling, ultrasonic treatment, and intercalation of inorganic molecules (e.g., NH_3, H_2O, and CO_2) and polymer PEO between $V_3O_8^-$ layers.[6,12,13] For example, Kumagai et al.[12] reported that ultrasonic treatment of LiV_3O_8 had the advantages of both higher discharge capacity (62% higher than that of the starting LiV_3O_8) and better cycling performance. West et al.[14] obtained a finely dispersed form of LiV_3O_8 through dehydration of aqueous lithium vanadate gel, and the synthesized LiV_3O_8 showed a high capacity and good reversibility. It is true that these treatments did improve the electrochemical performance of LiV_3O_8, but they usually require more time and complicated equipment, and thus are not feasible in large-scale production.

Recently, microwave solid-state preparation as a novel method has been developed to prepare cathode materials for lithium batteries.[15] Since the microwave energy is absorbed by reactants or heating medium, uniform and rapid heating can be achieved, and thus the high temperature needed in a solid-state reaction can be obtained within several minutes. Microwave preparation has already been applied to synthesize a number of inorganic materials, such as carbides, nitrides, complex oxides, silicides, and zeolites, and so forth.[16] Generally speaking, the microwave synthesis method needs a shorter reaction time and a lower temperature than the traditional method. In addition, the microstructure and property of the materials prepared by different synthesis methods are quite different. Beneficial results and application were found with the materials prepared by microwave irradiation, and many researchers have reported the substitution of traditional solid-state synthesis by the microwave method.[17] For instance, Subramanian et al.[17b] prepared $LiCoO_2$

* To whom correspondence should be addressed. Fax: +86-258331776. Phone: +86-2583686393. E-mail: whou@nju.edu.cn.
[†] Nanjing University.
[‡] Fudan University.

10.1021/jp050448s CCC: $30.25
Published on Web 05/13/2005

TABLE 1: Reaction Conditions of Samples Prepared by the Microwave Method

sample	reaction temp and time (x^a)	actual exposure time/min
L30	297 °C, 30 min (4 s/22 s)	5.45
L60	420°C, 60 min (4 s/22 s)	10.91
L80	485 °C, 80 min (4 s/22 s)	14.54
L100	530 °C, 100 min (4 s/22 s)	18.18
ML30	540 °C, 30 min (8 s/22 s)	10.91
M20	593 °C, 20 min (13 s/22 s)	11.82
M25	769 °C, 25 min (13 s/22 s)	14.77
MH12	609 °C, 12 min (17 s/22 s)	9.27
H8	542 °C, 8 min (22 s/22 s)	8.00

[a] x is the duty cycle of the microwave reactor. $x = t_{on}/t_{cycle}$; t_{on} is the working-on time in every irradiation cycle and t_{cycle} is the time of one irradiation cycle.

by using the microwave solid-state method, and the synthesized material demonstrated remarkable electrochemical performance.

In the previous paper, the heating behavior of a modified microwave oven and the crystal growth mechanism of layered compounds in the microwave field have been discussed.[18a] Here, we report the microwave solid-state synthesis of LiV_3O_8 and its electrochemical properties. The effect of microwave irradiation time and power on the microstructure and electrochemical property of LiV_3O_8 is discussed in detail. For clarifying the structure and morphology of LiV_3O_8 prepared under different conditions and their relationships with electrochemical performance, the samples are characterized and studied by X-ray diffraction (XRD), Fourier transform infrared (FTIR) and Raman spectroscopy, scanning (SEM) and transmission (TEM) electron microcopy, the BET surface area and four-probe DC method, and electrochemical impedance spectroscopy (EIS). The electrochemical performance of LiV_3O_8 as a cathode material in lithium secondary batteries has also been examined.

2. Experimental Section

2.1. Preparation of Layered LiV_3O_8 Material. The modified microwave reaction system was designed on the basis of a domestic microwave oven (National MN-MX26WF, frequency 2.45 GHz, maximum power 800 W, multimode oven).[18a] The temperature of the reaction system during irradiation was monitored online by using a sheathed Pt−Rh thermocouple connected with a computer. A 42 g sample of graphite powder (<30 mm) was used as the secondary heater, sealed in a 50 mL alumina vessel. The vessel was placed inside the well-insulated cavity with Kaowool. The alumina crucible loaded with 3 g of reactants was placed in the center of the secondary heater. A mode stirrer (a reflective and fan-shaped paddle) was used to ensure that the average field experienced by the sample was approximately the same in all directions.[18b] In the upper part of the crucible, there was a vent hole to air to ensure that the expected oxidation of vanadium in LiV_3O_8 could be obtained. The starting materials $LiOH{\cdot}H_2O$ and V_2O_5 were mixed in a stoichiometric ratio, and then irradiated at different irradiation time and power (L: the lowest power, ML: the middle lower power, M: the middle power, MH: the middle higher power, and H: the highest power), and finally allowed to cool in the microwave cavity. All the reagents were analytical grade without any pretreatment. The relevant experimental details are listed in Table 1. For comparison, LiV_3O_8 was also prepared by traditional solid-state reaction with use of an electric furnace according to the literature.[11] The stoichiometric mixture of $LiOH{\cdot}H_2O$ and V_2O_5 was heated at 650 °C for 10 h, and the obtained sample was termed CP650.

2.2. Characterization. The X-ray diffraction patterns were recorded on a ARL X'TRA X-ray diffractometer operated with Cu Kα radiation and Ni filter (the scan rate was 1 deg/min, the step size was 0.05°). FTIR and Raman spectra were obtained at room temperature on a Bruker VECTORTM 22 and a JY HR800 spectrometer, respectively. The morphology was investigated with a scanning electron microscope (SEM, Hitachi-X650 microscope, 20 kV) and a transmission electron microscope (TEM, JEOL JEM-200CX, 200 kV). BET surface area, pore diameter, and pore volume were obtained from N_2 adsorption isotherms measured at liquid nitrogen temperature with a Micromeritics ASAP-2010 instrument.

2.3. Electrochemical Testing. The Nyquist plots were recorded by using the Princeton M398 Electrochemical Impedance System between the frequencies of 0.1 Hz and 100 kHz at room temperature. The sandwiched test cell was assembled as Au|sample disk|Au, and the impedance data were fitted by using Z-View software from Scribner Associates, Inc. Variable-temperature conductivity was obtained by the four-probe DC method at N_2 atmosphere, and the chamber was placed in a thermostatic bath to control the temperature of the samples. The sample LiV_3O_8 was sufficiently ground and pressed at a pressure of 60 MPa for 10 min, and then the sample disk was placed between two electrodes of Au sheets. At every testing temperature, the temperature was kept constant for 30 min.

Electrochemical charge−discharge cycle performance of the samples was evaluated in model CR2025 coin cells. The composite cathode consisted of active LiV_3O_8 material as-prepared, acetylene black, and poly(tetrafluoroethylene) at a weight ratio of 80:15:5. The mixture was coated onto a nickel net, pressed into a disk, and then dried under vacuum at 95 °C for 15 h. This disk and a foil of lithium metal were used as the positive and negative electrodes, respectively. The separator was a Celgard 2300 membrane. The 1.0 M solution of $LiPF_6$ in anhydrous ethylene carbonate and dimethyl carbonate (the volumetric ratio was 1:1) was used as electrolyte (Merck). The charge−discharge cycling was galvanostatically tested at a current density of 0.2 mA/cm^2 (or 15 mA/g) at room temperature in a voltage range from 1.8 to 4.0 V.

3. Results and Discussion

3.1. Heating Behavior in the Microwave Field. The reactants $LiOH{\cdot}H_2O$ and V_2O_5 could only absorb a small amount of microwave at a relatively low temperature, and were not able to generate the high temperature needed in the solid-state reaction.[19] Therefore, a dual crucible system was devised by using graphite powder as the heating medium to achieve the high temperature. The sample was not completely surrounded by the secondary heater of graphite, and there was a vent hole to air in the upper part of the sample holder. After the microwave penetrated the vessel of the secondary heater, the microwave power dissipated to the reactants was greatly decreased, but was still enough to accelerate the solid-state reaction and complete it in several minutes. Periodically terminating the irradiation in every cycle led to the fact that the efficiency of microwave energy converted to heat energy was not the same at different microwave power (controlled by the duty cycle x). Both the temperature variation and heating rate of the reaction system were found to be closely associated with the microwave power.[18a] Therefore, the layered compound LiV_3O_8 could be conveniently and successfully synthesized under suitable microwave irradiation conditions, such as reaction temperature and irradiation power (see Table 1).

3.2. X-ray Diffraction Studies. The XRD patterns of samples synthesized at the lowest microwave power (i.e., the lowest

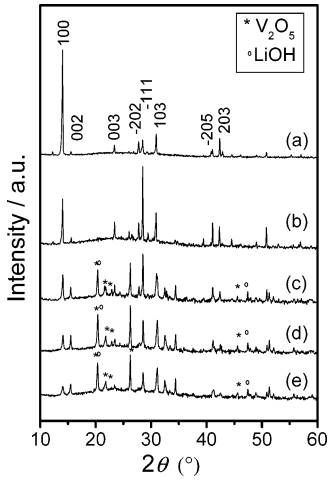

Figure 1. XRD patterns of LiV_3O_8 prepared by conventional method (a) CP650 and at the lowest irradiation power for different irradiation times: (b) 100, (c) 80, (d) 60, and (e) 30 min.

heating rate) for different irradiation times are shown in Figure 1. It can be seen that the materials irradiated for a relatively short time (30, 60, and 80 min) presented the peaks from both phases of product and reactants, indicating that the irradiation time and corresponding temperature attained in the microwave field were still not sufficient to form a pure product phase. For example, after irradiation for 30 min, the relative reaction temperature was only 297 °C and there were strong peaks (2θ = 20°, 34°, and so forth) arising from unreacted V_2O_5, but the formation of LiV_3O_8 was clearly in evidence. Along with the increase of irradiation time, the intensities of V_2O_5 peaks decreased while those of LiV_3O_8 increased. After irradiation for 100 min, it was showed that all peaks of L100 (Figure 1b) corresponded to the pure phase of LiV_3O_8 (JCPDS: 72-1193), and were in good agreement with those of the sample prepared by the traditional method (Figure 1a). The major difference between the samples prepared at different irradiation time (i.e., different reaction temperature) and by the traditional method was the relative intensity of some peaks of LiV_3O_8. For example, the intensity of crystal plane (100) increased while that of (002) decreased along with the increase of irradiation time. Compared with the traditional method, the microwave solid-state reaction was too rapid to have the chance of forming ordered phases, therefore, the small crystallites, low crystallinity, and different crystallite orientation were present, which gave rise to the broad and weak diffraction peaks.

The XRD patterns can also be used to reflect the conversion of reactants during the microwave irradiation. The plot of conversion vs reaction time and temperature is shown in Figure 2. It can be seen that the reaction conversion was mainly controlled by the reaction temperature, and was very low at a relatively low temperature (less than 420 °C). For example, the reactants were only converted 10% (from 40% to 50%) in the time range of 30 to 60 min (the corresponding reaction temperature achieved was between 297 and 420 °C). By comparison, the net increase in the conversion was 35% (from 65% to 100%) in the time range of 80 to 100 min (the corresponding reaction temperature achieved was between 485 and 530 °C).

The XRD patterns of LiV_3O_8 synthesized at five different irradiation powers are presented in Figure 3. These samples showed the same peaks with a layered lattice corresponding to the LiV_3O_8 structure (JCPDS: 72-1193). By comparison, the samples MH12 and H8 prepared at the relatively higher irradiation power had sharper diffraction peaks, and therefore

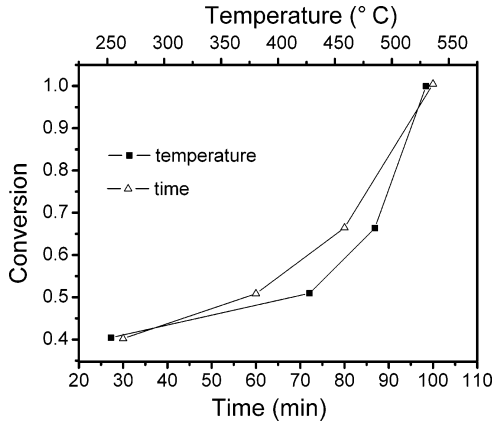

Figure 2. Plots of reaction conversion vs irradiation time and corresponding reaction temperature at the lowest microwave power (the conversion was measured by the intensity of the (100) peak of samples with respect to that of sample L100).

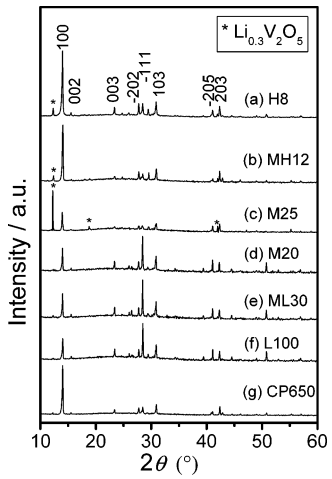

Figure 3. XRD patterns of LiV_3O_8 prepared with different microwave irradiation conditions and by conventional method.

TABLE 2: Lattice Parameters of LiV_3O_8 Synthesized with Different Irradiation Conditions

sample	*a*/Å	*b*/Å	*c*/Å	β	d_{100}/Å	d_{-111}/Å	I_{100}/I_{-111}
CP650	6.6146	3.5800	11.8943	107.6670	13.904	28.341	5.61
L100	6.6611	3.5980	12.0036	107.7555	14.038	28.488	0.65
ML30	6.6589	3.5973	12.0010	107.7568	14.004	28.454	0.64
M20	6.6619	3.5979	11.9999	107.7441	13.987	28.437	0.68
MH25	6.6941	3.5942	11.9343	107.8346	13.936	28.386	3.31
MH12	6.6635	3.5988	12.0066	107.8122	14.055	28.477	5.10
H8	6.6509	3.5961	12.0021	107.7781	13.994	28.443	4.21

a higher crystallinity. These experimental facts also confirmed that the pure phase of LiV_3O_8 could be synthesized in a very short time with the precondition that the needed reaction temperature was achieved. For example, LiV_3O_8 could be synthesized within 8 min at the highest microwave power (duty cycle, $x = 1$), and the corresponding reaction temperature was 542 °C. However, for the materials irradiated at a relatively higher microwave power (Figure 3a,b) or at a very high reaction temperature of 769 °C (Figure 3c), there was evidence of a small amount of $Li_{0.3}V_3O_8$. There were two reasons for the presence of $Li_{0.3}V_3O_8$. First, the ratio of Li:V at some local areas was not 1:3, because the reaction was too rapid to allow Li^+ ions to diffuse sufficiently. Second, part of reactant LiOH was volatilized or part of LiV_3O_8 was decomposed to the lithium-lacking material of $Li_{0.3}V_3O_8$ at a very high reaction temperature, such as 769 °C in the sample M25.

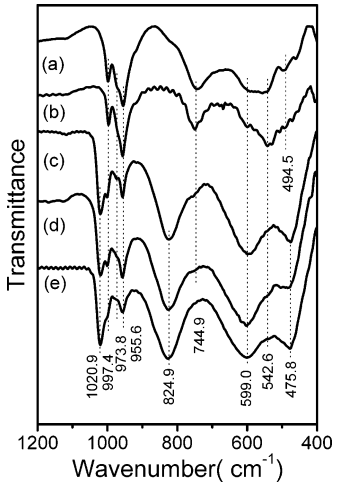

Figure 4. FTIR spectra of LiV_3O_8 prepared by conventional method (a) CP650 and with different irradiation times at the lowest microwave power: (b) 100, (c) 80, (d) 60, and (e) 30 min.

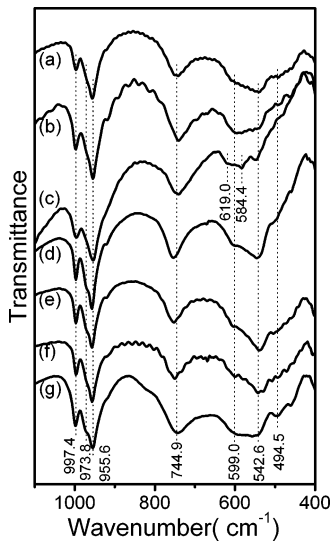

Figure 5. FTIR spectra of LiV_3O_8 prepared with different microwave irradiation conditions: (a) H8, (b) MH12, (c) M25, (d) M20, (e) ML30, (f) L100, and by conventional method (g) CP650.

The main difference of XRD patterns in the samples prepared at different irradiation powers was their relative intensities of the characteristic peaks. The lattice parameters of these materials were calculated by using the software of Unit cell with the function of zeroshift,[20] and are listed in Table 2. The calculated parameters were similar in all samples except for M25, which was prepared at a very high temperature of 769 °C. The intensity ratio of I_{100}/I_{-111} in the samples prepared at the relatively low irradiation power was much smaller than that prepared at the higher irradiation power, indicating that the preferential growth of some crystal planes was quite different at different irradiation powers.

3.3. FTIR and Raman Spectra Studies. The FTIR spectra of the samples prepared under different irradiation conditions are shown in Figures 4 and 5, respectively. The structural difference in the samples prepared by the traditional method and under different microwave irradiation conditions was mainly reflected by the V═O double bond peaks in the range of 1050−900 cm^{-1}. There are three short V═O bonds in the LiV_3O_8 crystal cell, and the corresponding bond lengths are 1.586, 1.584, and 1.583 Å, respectively.[21a] Therefore, the IR peaks at 955.6, 973.8, and 997.4 cm^{-1} could be assigned to the three short V═O bonds in the LiV_3O_8 crystal cell. The stretching vibrations

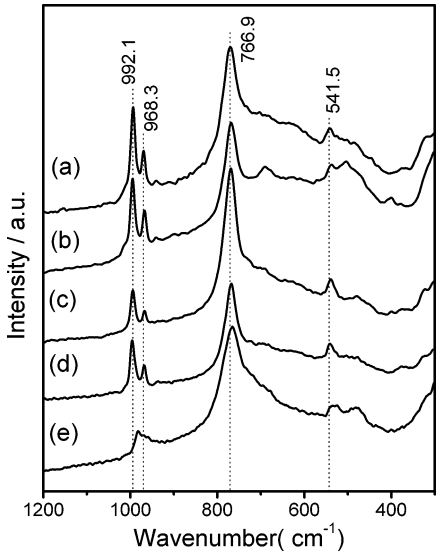

Figure 6. Raman spectra of LiV_3O_8 prepared by conventional method (a) CP650 and with different irradiation times at the lowest microwave power: (b) 100, (c) 80, (d) 60, and (e) 30 min.

of V−O−V appeared at 744.9 cm^{-1} and the peaks between 600 and 400 cm^{-1} were attributed to the bending vibrations of V═O and V−O−V.[21b,c]

At the lowest irradiation power, it can be seen in Figure 4 that the intensities of the peaks from unreacted V_2O_5 at 1020.9 [ν(V═O)], 824.9 [ν(V−O−V)], and 476.8 cm^{-1} [δ(V−O−V)][22b] decreased gradually along with the increase of irradiation time. After irradiation for 100 min, the sample L100 showed the same FTIR peaks as that prepared by the traditional method. This further confirmed that the formation of LiV_3O_8 needed a certain thermodynamic condition though microwave irradiation could accelerate the reaction. As shown in Figure 5, at the other microwave powers, the same phase of LiV_3O_8 could be rapidly formed while the reaction temperature was proper. The intensity and position of some peaks showed a little difference due to the dissimilar crystal growth behavior at different irradiation power. For example, the fine structure of three short V═O bonds in the LiV_3O_8 crystal cell was gradually not conspicuous along with the increase of irradiation power. The peak of ν(V−O−V) (744.9 cm^{-1}) showed a blue shift in the samples L100, ML30, and M20, and a red shift in the samples MH12 and H8 by comparison with that of CP650. On the other hand, the sample M25, which was prepared at a very high temperature (769 °C), presented a structure of lithium-lacking material $Li_{0.3}V_2O_5$ (see Figure 3c), and the peaks at 619.0 and 584.4 cm^{-1} were attributed to V−O stretching vibrations of $Li_{0.3}V_2O_5$ (Figure 5c).[22a,b]

The Raman spectra of the samples prepared under different irradiation conditions are shown in Figures 6 and 7, respectively. The Raman bands of LiV_3O_8 at 992.1 and 968.3 cm^{-1} could be assigned to the V═O stretching vibrations of VO_5 pyramids, and the band at 766.9 cm^{-1} was likely to be related to the atomic motions of corner-sharing oxygen among the VO_6, VO_5, and LiO_6 polyhedrons.[22c] At the lowest microwave power, the peaks appeared at the same positions in the samples synthesized for different irradiation times (Figure 6). Along with the increase of irradiation time and reaction temperature, the intensity of peak ν(V═O) increased gradually. At the other higher irradiation powers, the samples of M20, M25, MH12, and H8 showed a notable decrease in the intensity of the peak at 968.3 cm^{-1}, and the shift of some Raman peaks (Figure 7a−d). For example, the V═O stretching vibration (992.1 cm^{-1}) of VO_5 bipyramids

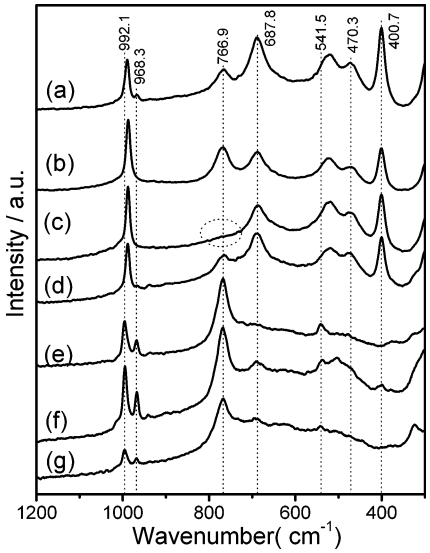

Figure 7. Raman spectra of LiV_3O_8 prepared under different microwave irradiation conditions: (a) H8, (b) MH12, (c) M25, (d) M20, (e) ML30, (f) L100, and by conventional method (g) CP650.

was shifted about 4 cm^{-1}, and the vibrations of B_{1g} and A_g symmetry species (541.5, 470.3 cm^{-1}) were shifted more than 20 cm^{-1}. It might be due to the rapid formation of VO_5 and VO_6 polyhedrons, and thus a little distortion of the crystal cells.[22c] Moreover, the intensity ratio of the two peaks at 992.1 and 766.9 cm^{-1} in samples M20, M25, MH12, and G8 prepared at a relatively high irradiation power was higher than that in samples L100 and ML30 prepared at a lower irradiation power. This indicated that the formation rate of VO_5 and VO_6 polyhedrons of $V_3O_8^-$ layers was much faster than the superposition rate of $V_3O_8^-$ layers linked by the interlayered Li^+ ions. At a very high temperature of 769 °C, the Raman peak at 766.9 cm^{-1} disappeared in sample M25, because the interlayered lithium ions were not enough to form the corner link among VO_5, VO_6, and LiO_6 polyhedrons. In addition, it should be noted that the peak at 400.7 cm^{-1} of $Li_{0.3}V_2O_5$ appeared, and it might be due to the rapid formation of $V_3O_8^-$ layers and the insufficient diffusion of Li^+ ions. Therefore, a too high irradiation power and temperature was disadvantageous to form the pure phase of LiV_3O_8 in the microwave field.

In general, the main peaks were the same in both IR and Raman spectra for the samples prepared by the traditional method and under different microwave conditions. However, the relative intensity and position of some peaks in Raman spectra showed a little difference. As is well-known, the scattering behavior and peak intensity of Raman spectra are usually affected by the thin layer structure of layered compounds with different grain boundaries and curvature.[23] The following SEM and TEM images (Figures 8 and 9) also showed that the morphology and grain size of the samples prepared under different conditions were quite different.

3.4. Surface Morphology and BET Surface Area Studies. As shown in Figures 8a and 9a, the sample prepared by the traditional method presented big and ordered crystals because of the high reaction temperature, long reaction time, and few disturbances during crystal growth. By comparison, the microwave synthesis method required a much shorter time and lower temperature to complete the solid-state reaction.

The SEM and TEM micrographs of LiV_3O_8 synthesized under different irradiation conditions are shown in Figure 8b−i and Figure 9b−i. At the lowest irradiation power, the divisions between the particles of sample L100 prepared at a relatively high temperature (i.e., long irradiation time) were more clear than those of samples L30 and L80 prepared at the lower temperature, indicating that a high synthesis temperature was beneficial to form more independent particles in the microwave field. An increase of crystallinity with the irradiation time was observed in Figure 8b−d and Figure 9b−d. After irradiation for 100 min (the corresponding reaction temperature reached 530 °C), the SEM and TEM images of sample L100 presented a relatively high crystallinity and big crystals that were composed of some curved thin nanosheets (the size of one nanosheet was estimated as 4.5 μm × 1.2 μm × 3 nm from Figure 9d). Because microwave irradiation not only promoted the ion diffusion but also decreased the reaction activation energy, the crystallites of LiV_3O_8 could be formed quickly at a relatively short irradiation time. This was confirmed by the same SAED analysis results (the inset images of Figure 9b−d). However, these crystallites still need enough time to grow bigger and more regular.

At the other irradiation powers, the samples presented disordered and bar-like crystals (Figure 8e−i). The samples M20, MH12, and H8 exhibited irregular bar-like particles (Figure 8h,i) whose sizes were widely distributed. The largest one had its longest side as long as 10 μm and the smallest one had its longest side less than 1 μm. The higher the irradiation power was, the smaller and more irregular were the crystals formed. For example, irregular and small crystals were formed in samples MH12 and H8 at the highest irradiation power in contrast with the sheetlike crystals of L100 and ML30 (Figure 8d,e). A similar result was also demonstrated in their TEM images (Figure 9). Especially, at the highest irradiation power, the TEM image (Figure 9i) of H8 presented a nanorod (about ϕ 70 nm) structure. The different crystal morphology of the samples revealed that the crystal growth was preferential at a certain crystal axis and plane in the microwave field.

The different morphology of crystals formed at different irradiation time and irradiation power was mainly due to the pondermotive force that acted at the interfaces and cavities to bring about a rapid growth of the grains and a systematic elimination of porosity.[16e] It is now established that microwave fields are very intense at interfaces, surfaces, and cavities during irradiation.[24] During the formation of materials, in particular, layered metal oxides, the pondermotive effect was responsible for the rapid growth along the layers. For example, with the increased irradiation time and reaction temperature, the particles of L100 became larger and more crystallized, and finally formed a floppy superposition structure of nanosheets that was greatly different from the ordered morphology of LiV_3O_8 prepared by the traditional method. On the basis of the theory of crystal chemistry, the growth of basic cells of crystal involves coordination polyhedron according to the relationship between the crystallographic orientation and crystal configuration. Actually, there may be different crystal configurations under different physical and chemical conditions, such as irradiation power (i.e., heating rate).

LiV_3O_8 has a monoclinic structure with the space group $P2_1/m$, and is composed of two basic structure units (VO_6 octahedron and VO_5 distorted trigonal bipyramid). The $V_3O_8^-$ layers are held together through the interaction with the interlayered lithium ions (Figure 12).[21a] The polyhedrons grown in the microwave field and by the traditional method could be connected to form the basic cells with different construction and dimensionalities, which were reflected in the crystal configurations. The superposition of basic cells in different dimensionalities had different stability, which directly influenced

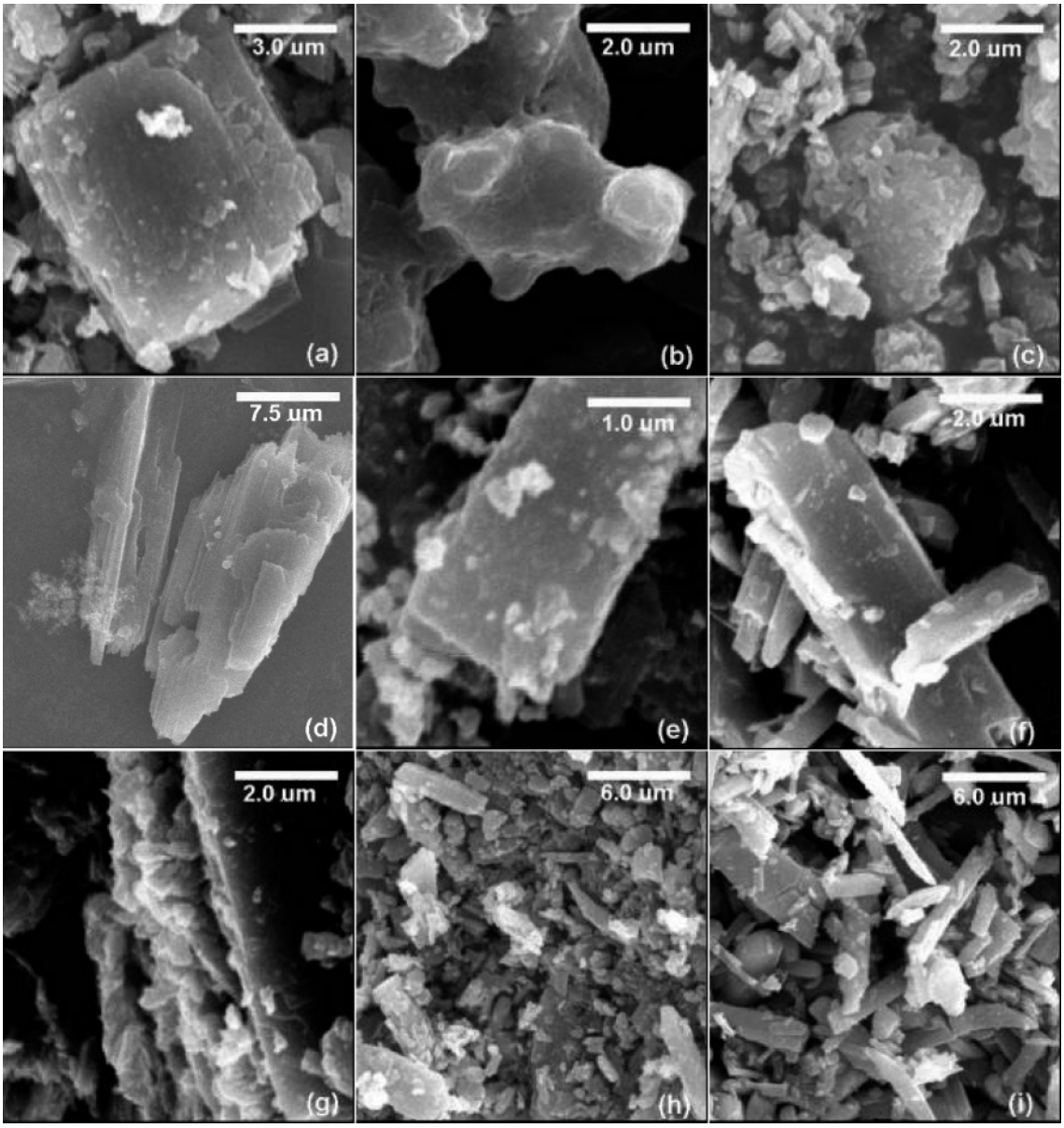

Figure 8. SEM images of LiV_3O_8 prepared by conventional method (a) CP650, and with different microwave conditions: (b) L30, (c) L80, (d) L100, (e) ML30, (f) M20, (g) M25, (h) MH12, and (i) H8.

the growth rate of each family of crystal planes. The crystal growth of the layered materials in the microwave field might be briefly proposed as follows: the crystallites of the product were quickly formed at first, and then the extended growth rate of the polyhedrons onto one monolayer was much faster than the superposition rate of monolayers, therefore the nanosheet structure of LiV_3O_8 (such as L100) was preferentially formed in the microwave field. At the higheset irradiation power, this effect was more in evidence as the nanorod was formed.

Generally, the floppy morphology and high surface area of the electrode materials are beneficial to the intercalation/deintercalation of Li^+ ions, and can lead to a high discharge capacity and good cycle ability.[25] The BET surface area, pore size, pore volume, and average grain size of the samples prepared under different conditions are summarized in Table 3. At the lowest irradiation power, because the samples irradiated for 30 and 80 min presented random structure and aggregation of microcrystals respectively, the high pore size and pore volume of L30 and L80 could be attributed to the interstice among the adjacent LiV_3O_8 microcrystals. When the irradiation time was increased up to 100 min, the pure phase of LiV_3O_8 was obtained and there was an observed increase in grain size, therefore its pore size, pore volume, and BET surface area were lower than those of L30 and L80. Due to the floppy superposition structure of nanosheets, the surface area of L100 (3.68 $m^2 \cdot g^{-1}$) was higher than that of CP650 (2.69 $m^2 \cdot g^{-1}$) with the ordered structure. At the other higher irradiation powers, the average particle size and BET surface area decreased rapidly along with the increase of irradiation power. The surface area of the electrode material always has a direct effect on the electrochemical performance.[17b]

3.5. Electrochemical Studies. Variable-temperature conductivities of LiV_3O_8 synthesized at different irradiation conditions are shown in Figure 10. At the lowest irradiation power, the sample L100 had the highest conductivity at a temperature range of 22−400 °C. This might be due to its floppy superposition structure and high BET surface area. At a relatively lower testing temperature (less than 130 °C), the conductivity of samples L30, L60, and L80 was much lower than that of the sample CP650 synthesized by the traditional method. When the testing temperature was increased, the conductivities of L30, L60, and L80 increased rapidly, and were beyond that of CP650. This might result from the fact that the transition phase of the samples

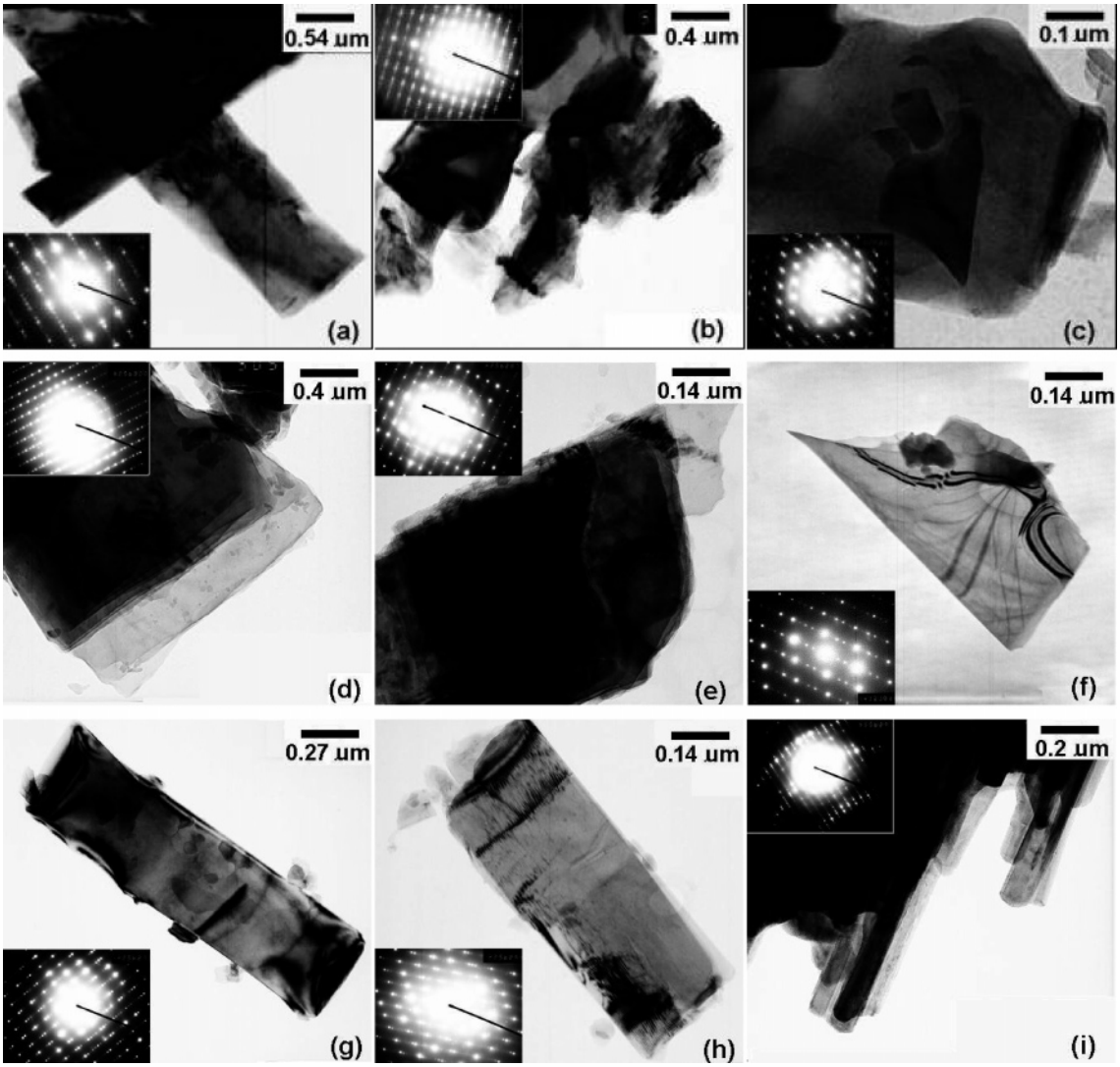

Figure 9. TEM images of LiV_3O_8 prepared by conventional method (a) CP650 and with different microwave conditions: (b) L30, (c) L80, (d) L100, (e) ML30, (f) M20, (g) M25, (h) MH12, and (i) H8. (The inset images are the typical SAED patterns.)

TABLE 3: The Average Particle Size, Pore Volume, and BET Surface Area of the Samples

sample	particle size/ μm	pore size/ Å	pore vol/ $cm^3 \cdot g^{-1}$	surface area/ $m^2 \cdot g^{-1}$
CP650	5.5	14.25	0.009396	2.69
L30	/	22.91	0.02480	4.28
L80	1.0	17.99	0.02647	5.83
L100	3.6	8.01	0.007580	3.68
ML30	3.1	12.61	0.004515	1.49
M20	2.6	16.82	0.006233	1.46
M25	/	17.36	0.006682	
MH12	1.5	72.43	0.005027	
H8	1.7	65.05	0.008639	0.53

formed in the microwave field for less than 80 min would be converted to the phase of LiV_3O_8, and the crystallites grew bigger on condition that the higher testing temperature was applied and kept constant for 30 min at every testing point. Moreover, the samples MH12 and H8 showed a lower conductivity than the samples L100 and M20 beyond room temperature (Figure 10, right). The possible reason was that the defection concentration in MH12 and H8 formed in a higher irradiation power was decreased at a relatively higher temperature during the long testing time.

The Nyquist plots recorded for LiV_3O_8 prepared by the traditional method and at different microwave power are shown

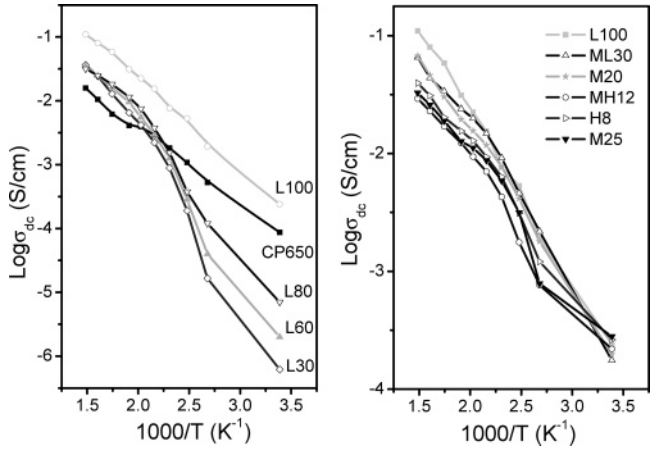

Figure 10. Variable-temperature conductivity of LiV_3O_8 prepared with different irradiation time at the lowest irradiation power (left) and at different irradiation power (right).

in Figure 11. The plots of LiV_3O_8 prepared by the microwave method for 30 and 80 min at the lowest irradiation power presented disordered data points, and could not be fitted, thus were not shown here. For the samples prepared at different microwave power, the impedance spectra mainly showed a high-frequency semicircle and a low-frequency spike.[17b] The imped-

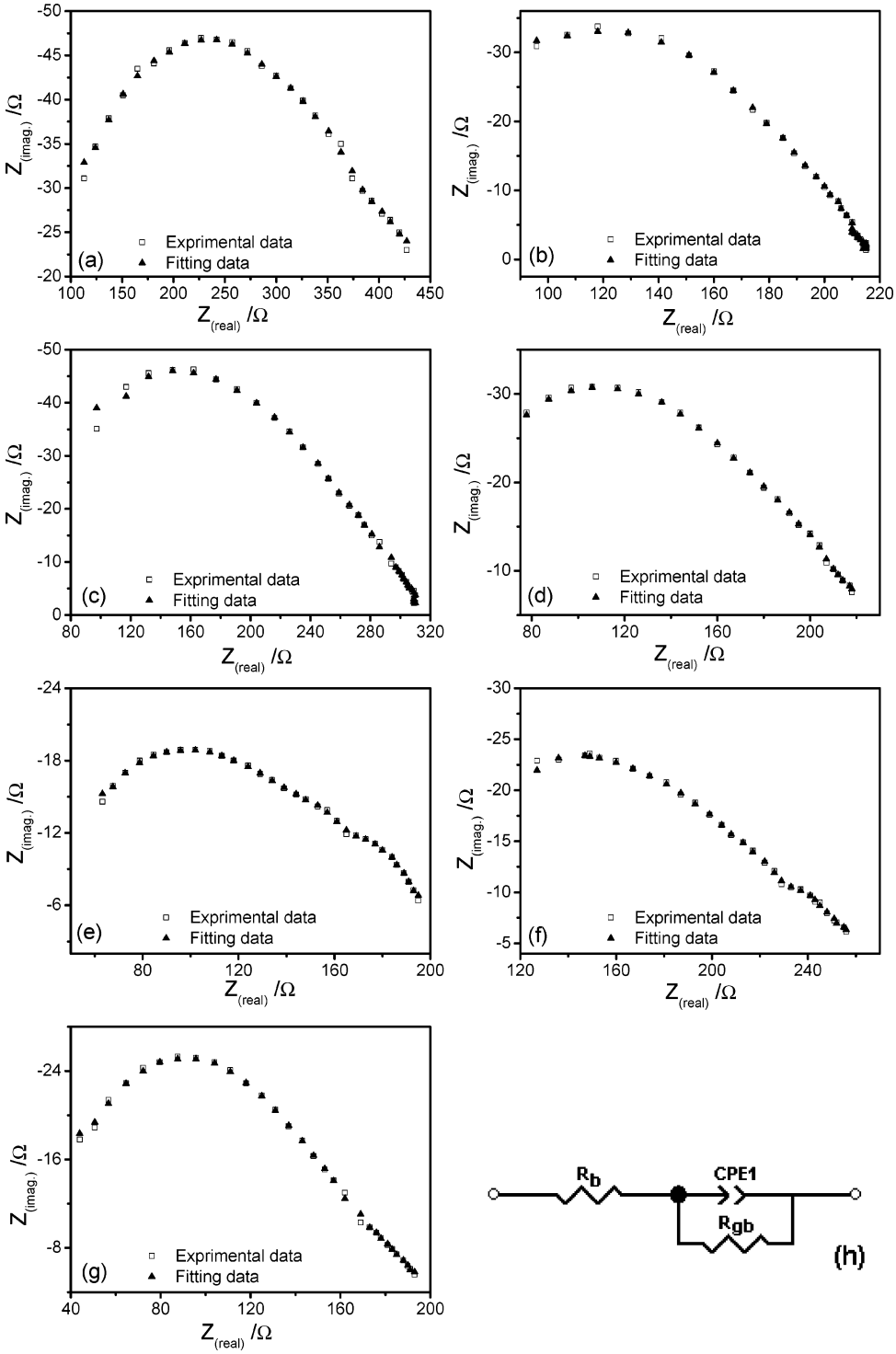

Figure 11. Nyquist plots of LiV_3O_8 synthesized under different conditions: (a) CP650, (b) L100, (c) ML30, (d) M20, (e) M25, (f) MH12, (g) H8, and (h) equivalent circuit model.

ance plots were fitted by using an equivalent circuit model (see Figure 11h), and the fitted impedance parameters are listed in Table 4. This model included the grain-body resistance (R_b), grain-boundary resistance (R_{gb}), and a constant phase element (CPE) attributed to the interface effect between the particles of LiV_3O_8.[26]

Two interesting results could be concluded from Table 4. First, all the calculated and experimental ionic conductivity of LiV_3O_8 prepared at different irradiation power was higher than that of CP650 prepared by the traditional method, and the same result was also demonstrated in their EIS fitting data. For example, R_b and R_{gb} of CP650 were the highest at 21.71 and 445.1 Ω, respectively, and relatively its calculated ionic conductivity was the lowest at 1.12×10^{-4} S/cm. This was attributed to the different crystal growth mechanism of layered material in traditional and microwave methods. In general, the crystal of LiV_3O_8 provides a two-dimensional channel for the transition of Li^+ ions. However, the different crystal configurations and local lattice distortion will affect the ionic transition route and grain-boundary resistance. Actually, there may be different crystal configurations and lattice distortion under different physical and chemical preparation conditions. In the traditional method, the crystals grew under high reaction temperature, long reaction time, and few disturbances, therefore

TABLE 4: Various Impedance Parameters, Ionic Conductivity, and Diffusion Coefficient of Li^+ Ions for LiV_3O_8 Synthesized with Different Microwave Conditions

samples	R_b/Ω	R_{gb}/Ω	CPE_1-$T^a/10^{-4}$ F	CPE_1-P^a/F	$\sigma_{RT}{}^b/10^{-4}$ S·cm^{-1} Calcd	$\sigma_{RT}{}^b/10^{-4}$ S·cm^{-1} Exptl	$D_{Li}{}^+/10^{-10}$ cm^2 s^{-1}
CP650	21.71	445.1	1.668	0.288	1.12	0.87	7.74
L100	16.96	198.0	0.275	0.416	2.45	2.40	8.02
ML30	11.33	297.4	0.423	0.381	1.71	1.75	2.46
M20	3.43	222.3	1.132	0.347	2.33	1.98	1.73
M25	0.91	211.8	5.396	0.225	2.47	2.80	3.13
MZ12	1.28	274.6	3.264	0.205	1.90	2.19	5.76
H8	0.63	193.4	2.001	0.327	2.71	2.63	4.68

[a] Capacitances for constant-phase element (CPE): T and P are the CPE parameters of the equation $Z = 1/[T(I^*\omega)^P]$ used to fit the depressed semicircle of the Nyquist plot.[17b] [b] σ_{RT} was the conductivity at room temperature. Calcd: The conductivity was calculated by the EIS data. Exptl: The conductivity was measured by the four-probe DC method.

big and ordered crystals presented (Figure 8a). By comparison, the crystals could be rapidly formed within a very short reaction time in the microwave field. Therefore, the samples showed disordered crystallites with different crystal size and random configuration, and simultaneously formed local lattice distortion with higher defection concentration. In the region of lattice distortion, both the interaction between Li^+ ions and negative layer $V_3O_8^-$ and the transition energy of Li^+ ions were decreased. Second, the grain body resistance (R_b) of samples LiV_3O_8 decreased along with the increase of irradiation power, but the grain-boundary resistance (R_{gb}) and the calculated and experimental ionic conductivity demonstrated diversity. For example, the samples prepared in the highest and lowest irradiation powers showed the lowest R_{gb} (198 and 193.4 Ω, respectively). Generally, the samples prepared under different conditions showed a relatively stable R_b resistance, and the resistance of samples was mainly dependent on the grain-boundary resistance (usually $R_b \ll R_{gb}$). Under different irradiation power, periodically terminating the irradiation in every cycle resulted in a different heating rate, and the crystal configuration of the samples would be affected. At the lowest irradiation power (the oven works in a cycle mode: 4s on 8s off), the crystallites of L100 were formed quickly in the period of irradiation working-on, and then preferential growth could occur along a certain crystal plane in the longer working-off time. At the highest irradiation power (continuous irradiation), the crystallites of H8 with a narrow distribution of crystal size were formed in a very short time, and these crystallites had a similar crystal conformation. Therefore, the samples L100 and H8 presented the lowest R_{gb} and the highest ionic conductivity. However, at the other irradiation power, because only a portion of the crystallites of samples ML30, M20, and MH12 were preferentially grown during a relatively shorter time in the period of irradiation working-off, the crystallites showed dissimilar crystal configuration with a relatively broader distribution of crystal size.

On the other hand, the local lattice distortion was changed under different irradiation power. At the lowest irradiation power, the lattice distortion was formed during irradiation working-on time, and crystallites grew along the lattice distortion under the longer working-off time. However, at the other irradiation power, because only a portion of the crystals grew along the distortion during the shorter time of irradiation working-off, the lattice distortion of the adjacent particles was dissimilar, and thus the samples ML30, M20, and MH12 showed a relatively higher R_{gb} and lower ionic conductivity.

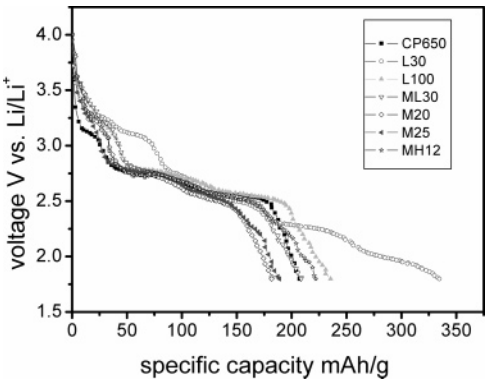

Figure 12. The first discharge curves of LiV_3O_8 prepared under different conditions. Discharge current density: 0.2 mA/cm^2 (15 mA/g)

Generally speaking, the grain surface (or here r^2) is a major contributor to the value of diffusion coefficient D. The diffusion coefficient (in Table 4) of LiV_3O_8 prepared with different conditions was calculated by using the formula $D_{Li} = (\pi f_T r^2)/1.94$, where r is the radius of the sample particles, and f_T is the frequency at which the impedance spectrum shows a transition from semi-infinite diffusion behavior to a finite-length behavior.[27] The r in the equation was an average value; however, the size distribution of samples ML30, M20, and MH12 was very uneven. Therefore, the diffusion coefficient D_{Li} decreased along with the increase of irradiation power and the decrease of BET surface area, but did not correspond to their calculated and experimental ionic conductivities.

To see how the microwave preparation conditions affect the electrochemical behavior, the first discharge capacities of samples prepared under different conditions are shown in Figure 12. The samples prepared at the lowest or middle higher irradiation power showed much higher discharge capacity (L30: 335 mAh/g, L100: 236 mAh/g, and MH12: 222 mAh/g) than the sample prepared by the traditional method (CP650: 207 mAh/g). However, the sample prepared at the medium irradiation power demonstrated a relatively lower discharge capacity (ML30: 208 mAh/g, and M20: 181 mAh/g). This could be explained by the strained $V_3O_8^-$ layers formed in the microwave field, because the Peierls energy was resisted by microwave irradiation energy.[28] The strained $V_3O_8^-$ layers were thermodynamically unstable compared with those perfect $V_3O_8^-$ layers of CP650. The sample L30 prepared at the lowest reaction temperature (297 °C) and the shortest reaction time (30 min) presented very tiny crystallites and high BET surface area, which resulted in the highest discharge capacity. The crystallites of LiV_3O_8 grew bigger with enough irradiation time (100 min) and a high temperature (530 °C). And during the longer period of irradiation working-off time, the interlayered Li^+ ions could diffuse sufficiently to lead to the formation of nanosheet superposition structure. Moreover, at the lowest irradiation power, the as-prepared crystallites presented a similar crystal configuration and a narrow distribution of crystal size. This structure was beneficial to the intercalation/deintercalation of Li^+ ions, thus sample L100 showed a higher capacity than CP650. By comparison, the crystallites prepared at a medium irradiation power had dissimilar crystal configurations and a broader distribution of crystal size; hence the intercalation/deintercalation of Li^+ ions in these crystals would suffer much interference, and relatively the electrochemical properties decreased.

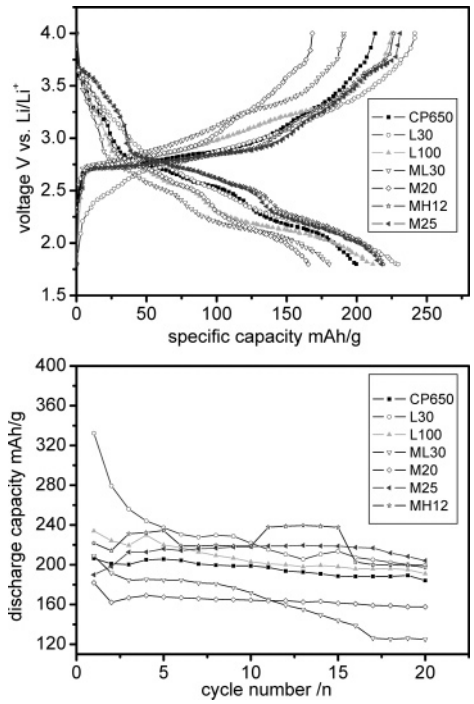

Figure 13. The eighth charge−discharge curves (upper) and variation in discharge capacity as a function of cycle number (bottom) for LiV_3O_8 prepared at different conditions. The charge−discharge cycles were carried out at a current density of 0.2 mA/cm^2 in the potential range from 1.8 to 4.0 V vs Li/Li$^+$.

The charge−discharge curves at the eighth cycle and the cycle performances of the samples prepared under different conditions are shown in Figure 13. During the intercalation/deintercalation process of Li^+ ions within the $V_3O_8^-$ layers, the crystallites of L30 were aggregated and the BET surface area would be decreased, and thus the sample L30 showed that the eighth discharge capacity decreased to 230 mAh/g. The discharge capacity of L30 decreased rapidly during the first four cycles, and then rather slowly as the structure became stable. However, the eighth discharge capacity of L100 only decreased a little to 210 mAh/g, and the sample L100 presented a good cycle performances within 20 cycles, indicating that the nanosheet superposition structure of L100 was stable during the process of charge−discharge. The sample ML30 had a similar first discharge capacity (208 mAh/g) with that of CP650, but its discharge capacity decreased greatly to 181 mAh/g at the eighth cycle. On the other hand, the samples prepared at a relatively higher irradiation power (M20, and MH12) and at a very high temperature (M25) presented a very stable cycle performance. In general, the crystal configurations and the distribution of crystal size were affected by the periodical irradiation, and relatively the samples demonstrated different electrochemical properties.

4. Conclusion

By using graphite powder as the heating medium to obtain the high temperature needed in the solid-state reaction, the pure phase of LiV_3O_8 was successfully synthesized at suitable irradiation time and power. At the lowest irradiation power, the conversion of reactants was mainly controlled by the reaction temperature. The morphology of the samples revealed the transition of random structure to higher crystallinity along with the increase of irradiation time. In the microwave field, because the extended growth rate of polyhedrons onto one monolayer was much faster than the superposition rate of monolayers, the floppy superposition structure of nanosheets (the size of one nanosheet was estimated as 4.5 μm × 1.2 μm × 3 nm) was preferentially formed at the lowest irradiation power, and this effect was more in evidence as the nanorod (about ϕ 70 nm) formed at the highest power.

The samples prepared at different irradiation power and time presented different sizes of crystallites with different crystal configuration and defection concentration in the microstructure, which affected ionic conductivity, first discharge capacity, and cycle performance. The sample L30 prepared at the lowest reaction temperature (297 °C) showed the highest discharge capacity (335 mAh/g), but then the discharge capacity decreased rapidly during the first four cycles. The sample L100 had a floppy superposition structure of nanosheets which provided a good two-dimensional channel for the transition of Li^+ ions and was stable during the intercalation/deintercalation process of Li^+ ions, therefore the high ionic conductivity, high discharge capacity, and good cycle performance were present. Moreover, the samples prepared at a relatively higher irradiation power and at a very high temperature presented a very stable cycle performance, because the as-prepared crystallites had a similar crystal configuration and a small distribution of crystal size. It was revealed that the electrochemical properties would be affected by the periodical irradiation.

Acknowledgment. This project was supported by the National Natural Science Foundation of China (Grant No. 29903005), the National Basic Research Program of China (Grant No. 2003CB615804), and the Modern Analysis Center of Nanjing University.

References and Notes

(1) Torardi, C. C.; Miao, C. R. *Chem. Mater.* **2002**, *14*, 4430.
(2) Pistoia, G.; Pasquali, M.; Tocci, M.; Maney, V.; Moshtev, R. V. *J. Power Sources* **1985**, *15*, 13.
(3) Nassau, K.; Murphy, D. W. *J. Non-Crystal. Solid* **1981**, *44*, 297.
(4) Dai, J. X.; Li, S. F. Y.; Gao, Z. Q.; Siow, K. S. *J. Electrochem. Soc.* **1998**, *145*, 3057.
(5) Scrosati, B.; Selvaggi, A.; Croce, F.; Gang, W. *J. Power Sources* **1988**, *24*, 287.
(6) Yu, A.; Kumagai, N.; Lee, J. Y. *J. Powder Sources* **1998**, *74*, 117.
(7) Kawakita, J.; Kato, T.; Katayama, Y.; Miura, T.; Kishi, T. *J. Power Sources* **1999**, *81*−*82*, 448.
(8) Pistoia, G.; Pasquali, M.; Wang, G.; Li, L. *J. Electrochem. Soc.* **1990**, *137*, 2365.
(9) Liu, G. Q.; Zeng, C. L.; Yang, K. *Electrochim. Acta* **2002**, *47*, 3239.
(10) Xu, H. Y.; Wang, H.; Sang, Z. Q.; Wang, Y. H.; Yan, H.; Yoshimura, M. *Electrochim. Acta* **2004**, *49*, 349.
(11) Wadsley, A. D. *Acta Crystallogr.* **1957**, *10*, 261.
(12) Kumagai, N.; Yu, A. *J. Electrochem. Soc.* **1997**, *144*, 836.
(13) (a) Yang, G.; Hou, W. H.; Sun, Z. Z.; Yan, Q. J. *J. Mater. Chem.* **2005**, *15*, 1369. (b) Manev, V.; Momchilov, A.; Nassalevska, A.; Pistoia, G. *J. Power Sources* **1995**, *54*, 501.
(14) West, K.; Zachau-Christiansen, B.; Skaarup, S.; Saidi, Y.; Barker, J.; Olsen, I. I.; Pynenburg, R.; Koksbang, R. *J. Electrochem. Soc.* **1996**, *143*, 820.
(15) (a) Whitfield, P. S.; Davidson, L. J. *J. Electrochem. Soc.* **2000**, *147*, 4476. (b) Nissinen, T. A.; Kiros, Y.; Gasik, M.; Leskela, M. *Chem. Mater.* **2003**, *15*, 4974. (c) Nakayama, M.; Watanabe, K.; Ikuta, H.; Uchimoto, Y.; Wakihara, M. *Solid State Ionics* **2003**, *164*, 35. (d) Birnbiom, A.; Calame, J. P.; Carmel, Y. J. *Appl. Phys.* **1999**, *85*, 478.
(16) (a) Roy, R.; Agrawal, D.; Cheng, J. P. *Nature* **1999**, *399*, 668. (b) Rao, K. J.; Vaidhyanathan, B.; Ganguli, M.; Ramarkrishnan, P. A. *Chem. Mater.* **1999**, *11*, 882. (c) Gabriel, C.; Gabriel, S.; Grant, E. H.; Halstead, B. S. J.; Mingos, D. M. P. *Chem. Soc. Rev.* **1998**, *27*, 213. (d) Ramesh, P. D.; Rao, K. J. *Adv. Mater.* **1995**, 7177. (e) Panneerselvam, M.; Rao, K. J. *Chem. Mater.* **2003**, *15*, 2247.
(17) (a) Harpeness, R.; Gedanken, A.; Weiss, A. M.; Slifkin, M. A. *J. Mater. Chem.* **2003**, *13*, 603. (b) Subramanian, V.; Chen, C. L.; Chou, H. S.; Fey, T. K. *J. Mater. Chem.* **2001**, *11*, 3348. (c) Zhou, G. T.; Palchik, O.; Pol, V. G.; Sominski, E.; Koltypin, Y.; Gedanken, A. *J. Mater. Chem.* **2003**, *13*, 2607.

(18) (a) Yang, G.; Kong, Y.; Hou, W. H.; Yan, Q. J. *J. Phys. Chem. B* **2005**, *109*, 1371−1379. (b) Mingos, D. M. P.; Baghurst, D. R. *Chem. Soc. Rev.* **1991**, *20*, 1.

(19) In a microwave field, the reactant mixture for LiV_3O_8 was once directly irradiated without heating medium for 100 min at the lowest irradiation power and only reached 120 °C.

(20) Holland, T. J. B.; Redfern, S. A. T. *Mineral. Mag.* **1997**, *61*, 65.

(21) (a) Picciotto, de L. A.; Adendorff, K. T.; Liles, D. C.; Thackeray, M. M. *Solid State Ionics* **1993**, *62*, 297. (b) Tossici, R.; Marassi, R.; Berrettoni, M.; Stizza, S.; Pistoia, G. *Solid State Ionics* **1992**, *57*, 227. (c) Abello, L.; Husson, E.; Repelin, Y.; Lucaeau, G. *Spectrochim. Acta* **1983**, *39A*, 641.

(22) (a) Popović, Z. V.; Gajić, R.; Konstantinović, M. J.; Provoost, R.; Moshchalkov, V. V.; Vasil'ev, A. N.; Isobe, M.; Ueda, Y. *Phys. Rev. B* **2000**, *61*, 11454. (b) Vijayakumar, M.; Selvasekarapandian, S.; Kesavamoorthy, R.; Nakamura, K.; Kanashiro, T. *Mater. Lett.* **2003**, *57*, 3618. (c) Zhang, X.; Frech, R. *Electrochim. Acta* **1998**, *43*, 861.

(23) (a) Auvray, L.; Cotton, J. P.; Ober, R.; Taupin, C. *Physics* **1984**, *45*, 913. (b) Auvray, L.; Cotton, J. P.; Ober, R.; Taupin, C. *J. Phys. Chem.* **1984**, *88*, 4586.

(24) Freeman, S. A.; Booske, J. H.; Cooper, R. F. *Phys. Rev. Lett.* **1995**, *74*, 2042.

(25) Pereira-Ramos, J. P.; Baffier, N.; Pistoia, G., Eds. *Lithium Batteries*; Elsevier Press: Amsterdam, The Netherlands, 1994; p 298.

(26) Choi, Y. M.; Pyun, Y. H. *Solid State Ionics* **1999**, *99*, 173.

(27) Conway, B. E. *J. Electrochem. Soc.* **1991**, *138*, 1539.

(28) Weinheim, V. G., Eds. *Structure of Solids*; Willy-VCH Press: New York, 1993.